Direct Visualization of Laser-Driven Electron Multiple Scattering and Tunneling Distance in Strong-Field Ionization

Daniel D. Hickstein,[1] Predrag Ranitovic,[1,*] Stefan Witte,[1,2] Xiao-Min Tong,[3] Ymkje Huismans,[4] Paul Arpin,[1] Xibin Zhou,[1] K. Ellen Keister,[1] Craig W. Hogle,[1] Bosheng Zhang,[1] Chengyuan Ding,[1] Per Johnsson,[5] N. Toshima,[3] Marc J. J. Vrakking,[6] Margaret M. Murnane,[1] and Henry C. Kapteyn[1]

[1]*JILA and Department of Physics, University of Colorado at Boulder and NIST, Boulder, Colorado 80303, USA*
[2]*Institute for Lasers, Life and Biophotonics, VU University, De Boelelaan 1081, 1081 HV Amsterdam, The Netherlands*
[3]*Division of Materials Science, Faculty of Pure and Applied Sciences, University of Tsukuba, Ibaraki 305-8573, Japan*
[4]*FOM Institute AMOLF, Science Park 104, 1098 XG Amsterdam, The Netherlands*
[5]*Lund University, P. O. Box 118, SE-221 00 Lund, Sweden*
[6]*Max-Born-Institute, Max-Born Strasse 2A, D-12489 Berlin, Germany*

(Received 14 March 2012; published 16 August 2012)

Using a simple model of strong-field ionization of atoms that generalizes the well-known 3-step model from 1D to 3D, we show that the experimental photoelectron angular distributions resulting from laser ionization of xenon and argon display prominent structures that correspond to electrons that pass by their parent ion more than once before strongly scattering. The shape of these structures can be associated with the specific number of times the electron is driven past its parent ion in the laser field before scattering. Furthermore, a careful analysis of the cutoff energy of the structures allows us to experimentally measure the distance between the electron and ion at the moment of tunnel ionization. This work provides new physical insight into how atoms ionize in strong laser fields and has implications for further efforts to extract atomic and molecular dynamics from strong-field physics.

DOI: 10.1103/PhysRevLett.109.073004 PACS numbers: 32.80.Fb, 32.80.Rm, 34.80.Qb

When an atom or molecule is illuminated with a moderately intense femtosecond laser field ($\sim 10^{14}$ W/cm^2), an electron wave packet will tunnel ionize and accelerate in the field before being turned around by the field and returning to the parent ion. The returning electron can either recombine with the parent ion, releasing its kinetic energy as a high-energy photon [1–3], or can elastically scatter from the potential of the ion. The photons and electrons generated by these strong-field processes have the potential to probe the dynamic structure of molecules and materials on the subnanometer length scale and femtosecond-to-attosecond time scale. Several recent papers have suggested that structures seen in angle-dependent photoelectron spectra may be useful for determining time-resolved molecular structures [4], characterizing attosecond electron wave packets [5], and studying the dynamics of electron wave packet propagation [6]. However, despite extensive analyses [7–11], many features observed in angle-resolved photoelectron spectra still lack a simple physical explanation.

The recent development of midinfrared (mid-IR) femtosecond lasers [12] and angle-resolved detection schemes [13] has enabled new advances in visualizing strong-field physics. Electrons that are ionized in a mid-IR laser field reach higher velocities because of the larger ponderomotive energy, given by $U_P \propto I\lambda^2$, where I is the intensity and λ is the wavelength. The possibility of harnessing the high-energy electrons that are first ionized and then driven back to a molecule by a strong laser field has inspired several theoretical and experimental efforts to use strong-field ionization to probe molecular structure [4,14–16]. Recently, Huismans and co-workers [17] used 7 μm mid-IR lasers, in combination with angle-resolved detection, to observe angular interference structures in the photoelectron spectra. They presented a theoretical model that explains these structures based on the difference in the phase between two different paths that electrons can take to reach the same final momentum, one of which involves a laser-driven recollision of the electron with the ion. In another work, Blaga and co-workers [18] irradiated atoms and molecules with 1.7–3.4 μm lasers and discovered an unexpected spike in the (non-angle-resolved) photoelectron energy spectrum that they refer to as the low-energy structure. Subsequent papers [19–22] proposed various interpretations, but all agree that this low-energy structure arises from the rescattering of electrons by the parent ion.

In this work, we develop an intuitive model for understanding strong-field ionization as a simple superposition of plane and spherical photoelectron waves. This approach generalizes the standard 3-step model of strong-field ionization that has provided crucial physical insight into strong-field ionization [23,24] and high-harmonic generation [25,26]. We use this model to show that new interference structures, which we observe in the experimental photoelectron angular distributions generated by mid-IR lasers, are created by electron trajectories that scatter from the parent ion after passing by the ion several times. The

quantum phase accumulated by the electrons during their oscillatory path between ionization and rescattering is directly imprinted onto the photoelectron angular distribution. Thus, the shape and spacing of the interference structures directly correspond to the specific number of times the electron reencounters its parent ion before scattering strongly. Through an analysis of the energy cutoff of these newly observed structures, we show that when an atom is ionized by an intense laser field, the electron emerges at a finite distance from its parent ion. This distance corresponds to the far side of the quantum tunneling barrier. Our simple model allows us to uncover valuable physical insight into strong-field electron dynamics and provides an explanation for many of the features previously seen in experimental photoelectron distributions.

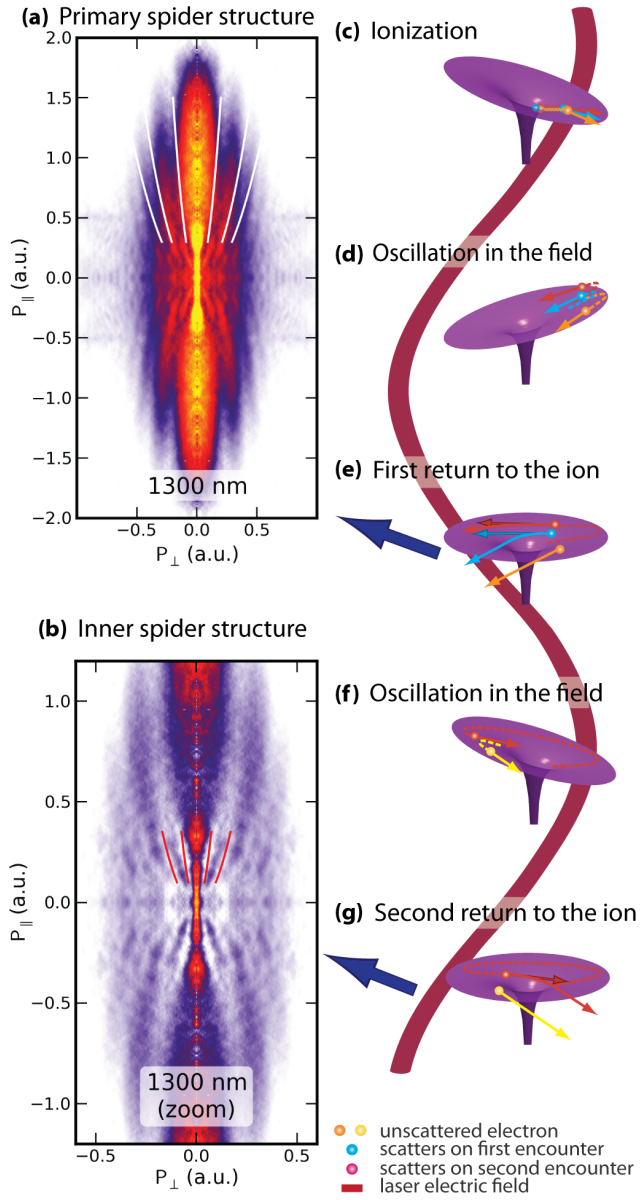

FIG. 1 (color online). (a) The photoelectron angular distribution resulting from the ionization of argon gas with a 1300 nm, 7.5×10^{13} W/cm^2, 40 fs laser pulse. The primary spider structure (minima shown with white lines) results from the interference between directly ionized electrons and those that are driven back to scatter from the Coulomb potential. (b) The newly observed inner structure (minima shown with red lines) results from electron trajectories that scatter from the Coulomb potential on their second reencounter with the ion and interfere with unscattered trajectories. (a)–(e) Simple laser-driven electron dynamics during ionization explain the primary and inner spider structures.

Our experimental apparatus consists of an ultrafast 30 fs Ti:sapphire laser and a velocity-map imaging photoelectron spectrometer. Nonlinear crystals and an optical parametric amplifier generate ultrafast pulses with wavelengths spanning 0.26 to 2 μm and durations of 40 fs. Spectra were recorded at various wavelengths between 0.26 and 2.0 μm, with intensities ranging from 5×10^{13} to 5×10^{14} W/cm^2 for xenon and argon gases. For driving wavelengths between 0.39 and 2.0 μm, we observe interference structures aligned along the laser polarization axis [Fig. 1(a)]. Huismans and co-workers [17] observed these structures and interpreted them in terms of an interference between laser-driven electron trajectories that recollide with the ion and electron trajectories that do not. In this Letter, we refer to these angular features as "spider structures" because of their resemblance to the body and legs of a spider. For driving laser wavelengths of 1.3 and 2 μm, we observe additional "inner spider" structures [Fig. 1(b)] at low final momenta that have more closely spaced fringes. Unlike other low-energy angular structures reported in the literature [27–29], these inner spider structures remain

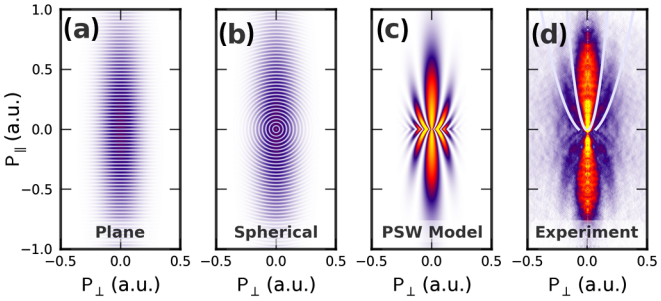

FIG. 2 (color online). The PSW model. The superposition of a plane wave (a) and a spherical wave (b) generates an interference pattern (c) that has the same shape as the spider structures. The phase of the plane wave is given by $\Psi_{\text{plane}} \propto e^{ikP_\parallel}$, while the phase of the spherical wave is given by $\Psi_{\text{spherical}} \propto e^{ikP_{\text{total}}}$, where $P_\parallel$ is the momentum parallel to the laser polarization, $P_{\text{total}} = \sqrt{P_\parallel^2 + P_\perp^2}$ is the total momentum, and k is the modulation frequency of the plane and spherical waves. Only the real part of the complex wave is shown in panels (a) and (b), while $|\Psi|^2$ is shown in panel (c). (d) The minima of the spider structure calculated using the plane-spherical model (white lines) match the experimental data across a broad range of wavelengths and intensities (shown: 1300 nm, 5×10^{13} W/cm^2, 40 fs driving laser).

remarkably robust to changes in the intensity of the driving laser.

To physically interpret both the inner and primary spider structures, we begin with the three-step (recollision) model of strong-field high-harmonic generation, which starts with tunneling ionization of an electron from the neutral atom in the presence of a strong laser field [Fig. 1(c)]. Next, the electron moves under the influence of the driving field, first being accelerated away from the parent ion and then driven back toward it [Fig. 1(d)]. Depending on the phase of the laser field when the electron tunnels, the electron may return to the vicinity of the parent ion, or it may drift away. Huismans and co-workers showed that the spider structures can be reproduced by assuming that electrons born with low transverse momentum can scatter elastically from the ion [Fig. 1(e)], a method referred to as the "generalized strong-field approximation" [17].

The plane-spherical wave (PSW) model (Fig. 2) further simplifies the generalized strong-field approximation model to its essential physics by treating the revisiting electrons as a simple plane wave and the rescattered electrons as a spherical wave. In the PSW model, the only thing that needs to be calculated is the spatial modulation frequency of the plane and spherical waves on the detector, i.e., the dependence of the phase of the electron on the final momentum. In the Lewenstein model [26,30], the phase of an ionized electron is $e^{-iS/\hbar}$, where S is the quasiclassical action, given by

$$S(p, t, t_b) = \int_{t_b}^{t} \left(\frac{p(t')^2}{2m_e} + I_p \right) dt', \tag{1}$$

where I_P is the ionization potential of the atom or molecule, m_e is the mass of the electron, t_b is the time the electron tunnels into the continuum, and $p(t')$ is the momentum. Thus, the probability of observing an electron at some position on the detector can be found by integrating all of the classical trajectories that reach the same final momentum and adding them coherently. In practice, Eq. (1) needs only be integrated up until the time when the electron rescatters from the ion, after which both electrons take identical paths to the detector. In the PSW model, the situation is further simplified because the calculation can be completed in just one dimension: along the component of electron momentum in the direction of the laser polarization direction ($P_\parallel$). By plotting the action versus $P_\parallel$ [Fig. 3(b)], we can estimate the modulation frequency as the slope of this line. This modulation frequency, in turn, determines the spacing of the interference fringes in the spider structure.

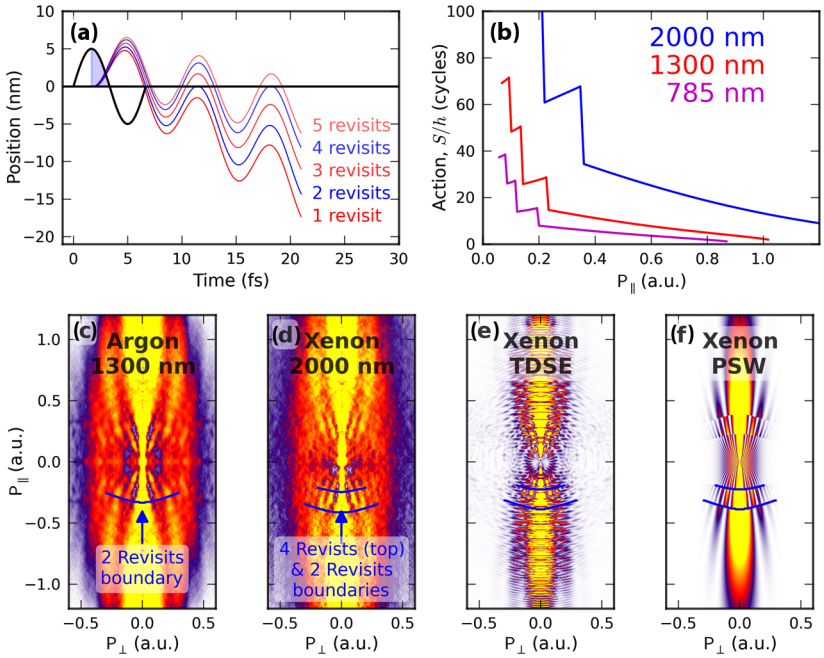

FIG. 3 (color online). (a) Depending on when an electron tunnels, it will be driven past the ion a specific number of times. (b) Quasiclassical action obtained by integrating each electron trajectory from when it is born to when it revisits the ion for the second-to-last time versus the final momentum parallel to the laser polarization ($P_\parallel$). The frequency of the plane and spherical waves is given by the slope of this graph. The "steps" at low momenta correspond to regions of multiple rescattering. (c) Experimental photoelectron distribution from argon ionized by a 1.3 μm, 7.5×10^{13} W/cm^2 laser shows a clear boundary between the high momentum region (one revisit) and the low-momentum region where scattering can take place during a subsequent revisit. (d) Photoelectron distribution from xenon using a 2.0 μm, 5×10^{13} W/cm^2 laser displays two boundaries that correspond to the second and fourth revisits. (e) Time-dependent Schrödinger equation (TDSE) calculations reproduce the low-momenta structures in xenon. (f) Single-cycle PSW model, including scattering on the first revisit (outer spiders) as well as the second and fourth revisits (inner spider structures).

This simple procedure generates interference patterns that quantitatively reproduce the spacing and shape of the spider structures seen in experimental data. As shown Fig. 1(a), the predicted minima are in excellent agreement with the experimentally observed interference minima. This agreement is achieved with no fitting parameters—the structures are generated from first principles with minimal computational effort. The calculation requires only the wavelength and intensity of the driving laser and the ionization potential of the atom. Importantly, the overall shape and spacing of the spider structures do not depend strongly on the structure of the atom or molecule. Nevertheless, the PSW model suggests that structural information will be encoded in the momentum-dependent ratio between the plane wave and the spherical wave.

In addition to reproducing the primary spider structures, the PSW model also offers a simple explanation for the inner spider structures. By examining the classical electron trajectories [Fig. 3(a)], it is clear that trajectories that arrive at the detector with low final momenta correspond to electrons that are ionized near the peak of the laser field and that can be driven past their parent ion more than once. Subsequent revisits of the ionized electron to the core take place with lower velocities, making scattering more likely. The PSW model allows us to easily compute the spacing of the spider structures that would result from scattering on the first, second, third, or subsequent revisit and compare this spacing to the experimental photoelectron angular distribution [Fig. 3(f)]. By carefully measuring the spacing of the inner spider structure in the experimental photoelectron spectra and comparing these measurements with the results of the simple PSW model [Fig. 1(g)], we conclude that scattering on the *second-to-last* reencounter (we observe scattering on the second revisit) plays the most significant role. A classical analysis of the electron trajectories [Fig. 3(a)] also predicts that there will be a sharp cutoff between electron trajectories that scatter from the ion on the first revisit and those that scatter on a subsequent revisit. The calculated spacing of the spider structure inside the first boundary [Fig. 3(f)] is approximately half the frequency of that outside, in good agreement with experiment [Fig. 3(c)].

The cutoff energies for various numbers of revisits can be easily calculated using classical mechanics [Figs. 3(c)–3(f)]. If we assume that electrons tunnel at $x = 0$, then electrons with kinetic energy greater than $0.09U_p$ will revisit only once, electrons with energy between 0.09 and $0.06U_p$ will revisit 3 times (scattering on the second revisit), and electrons with energy less than $0.06U_p$ will revisit five or more times (scattering on the fourth, or subsequent even-numbered revisit). However, the predicted position of the cutoff is slightly lower than that observed in the experimental photoelectron spectra unless the finite tunnel distance is taken into account. The tunnel distance results from the fact that electrons will tunnel into the continuum at a finite distance from the atom. This distance is dictated by the strength of the electric field and the ionization potential of the species [Fig. 4(a)]. At the peak of a laser field of intensity 5×10^{13} W/cm^2, the tunnel distance is on the order of 5 Å for most atoms. If this finite tunnel distance is considered, the classical boundaries move to slightly higher energies, and are in better agreement with the experimental data [Fig. 4(b), and Supplemental Material [31]). To our knowledge, this is the first example where the finite tunnel distance inherent in strong-field ionization can be extracted from an experimental observable.

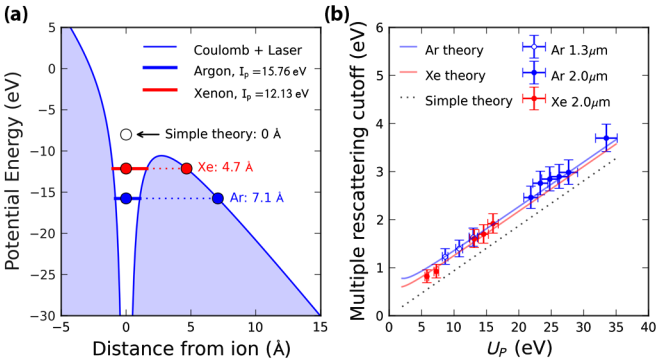

FIG. 4 (color online). (a) In the presence of a strong laser field (5×10^{13} W/cm^2), the atomic Coulomb potential is deformed, enabling tunnel ionization. (b) By examining the classical equations of motion, we plot the theoretical cutoff between trajectories that revisit the ion once and those that rescatter several times (lines). If the tunnel distance is included, the theoretically predicted multiple rescattering cutoffs agree with the experimentally observed cutoffs (points). The experimental intensity was calibrated from the $2U_P$ cutoff. The error in the energy of the multiple rescattering cutoff was assumed to be 0.02 atomic units of momentum.

In conclusion, by generalizing the well-known 3-step strong-field ionization model from 1D to 3D using a simple plane-spherical wave model, we can intuitively explain the experimental photoelectron angular distributions of atoms ionized in strong laser fields. We show that new low-energy features display clear signatures that an electron can pass by its parent ion more than once before strongly scattering from it. Furthermore, the data show that when an atom is ionized by an intense laser, the electron emerges at a finite distance from its parent ion that corresponds to the far side of the quantum tunneling barrier. These new observations and physical explanations will inform future studies that seek to extract femtosecond-resolved structural information from strong-field ionization.

The authors acknowledge support from the DOE Office of Basic Energy Sciences (AMOS program) and used facilities provided by the NSF Center for EUV Science and Technology. D. H. acknowledges support from the NSF under Grant No. DGE 0707432. S. W. acknowledges support from the Netherlands Organization for Scientific Research (NWO Veni Grant No. 680-47-402).

*To whom all correspondence (inquiry) should be addressed.
pranitovic@lbl.gov

[1] A. McPherson *et al.*, J. Opt. Soc. Am. B **4**, 595 (1987).
[2] M. Ferray, A. L'Huillier, X. F. Li, L. A. Lompre, G. Maunfray, and C. Manus, J. Phys. B **21**, L31 (1988).
[3] P. Agostini, F. Fabre, G. Mainfray, G. Petite, and N. K. Rahman, Phys. Rev. Lett. **42**, 1127 (1979).
[4] J. Xu, Z. Chen, A.-T. Le, and C. D. Lin, Phys. Rev. A **82**, 033403 (2010).
[5] J. Mauritsson *et al.*, Phys. Rev. Lett. **105**, 053001 (2010).
[6] G. Sansone *et al.*, Nature (London) **465**, 763 (2010).
[7] P. B. Corkum, Phys. Rev. Lett. **71**, 1994 (1993).
[8] W. Becker, A. Lohr, and M. Kleber, J. Phys. B **27**, L325 (1994).
[9] D. B. Milošević and F. Ehlotzky, Phys. Rev. A **58**, 3124 (1998).
[10] P. Salières *et al.*, Science **292**, 902 (2001).
[11] G. G. Paulus, F. Grasbon, H. Walther, R. Kopold, and W. Becker, Laser Phys. **12**, 262 (2002).
[12] G. Andriukaitis, T. Balčiūnas, S. Ališauskas, A. Pugžlys, A. Baltuška, T. Popmintchev, M.-C. Chen, M. M. Murnane, and H. C. Kapteyn, Opt. Lett. **36**, 2755 (2011).
[13] A. T. J. B. Eppink and D. H. Parker, Rev. Sci. Instrum. **68**, 3477 (1997).
[14] C. I. Blaga, J. Xu, A. D. DiChiara, E. Sistrunk, K. Zhang, P. Agostini, T. a. Miller, L. F. DiMauro, and C. D. Lin, Nature (London) **483**, 194 (2012).
[15] Y. Wu, H. Ye, and J. Zhang, Phys. Rev. A **84**, 043418 (2011).
[16] T. Morishita, A.-T. Le, Z. Chen, and C. D. Lin, Phys. Rev. Lett. **100**, 013903 (2008).
[17] Y. Huismans *et al.*, Science **331**, 61 (2010).
[18] C. I. Blaga, F. Catoire, P. Colosimo, G. G. Paulus, H. G. Muller, P. Agostini, and L. F. DiMauro, Nature Phys. **5**, 335 (2009).
[19] F. H. M. Faisal, Nature Phys. **5**, 319 (2009).
[20] C. Liu and K. Z. Hatsagortsyan, J. Phys. B **44**, 095402 (2011).
[21] C. Liu and K. Z. Hatsagortsyan, Phys. Rev. Lett. **105**, 113003 (2010).
[22] T.-M. Yan, S. V. Popruzhenko, M. J. J. Vrakking, and D. Bauer, Phys. Rev. Lett. **105**, 253002 (2010).
[23] M. Y. Kuchiev, JETP Lett. **45**, 404 (1987).
[24] H. B. Van Linden, V. D. Huevell, and H. G. Muller, in *Multiphoton Processes*, edited by S. J. Smith and P. L. Knight (Cambridge University Press, Cambridge, 1988).
[25] K. C. Kulander, K. J. Schafer, and J. L. Krause, in *NATO Advanced Science Institutes Series*, edited by J. Piraux, A. L'Huillier, and K. Rzazewski (Plenum Press, New York, 1993), Vol. 316, pp. 95–110.
[26] M. Lewenstein, P. Balcou, M. Y. Ivanov, A. L'Huillier, and P. B. Corkum, Phys. Rev. A **49**, 2117 (1994).
[27] A. Rudenko, K. Zrost, C. D. Schröter, V. L. B. de Jesus, B. Feuerstein, R. Moshammer, and J. Ullrich, J. Phys. B **37**, L407 (2004).
[28] T. Marchenko, H. G. Muller, K. J. Schafer, and M. J. J. Vrakking, J. Phys. B **43**, 095601 (2010).
[29] D. G. Arbó, S. Yoshida, E. Persson, K. I. Dimitriou, and J. Burgdörfer, Phys. Rev. Lett. **96**, 143003 (2006).
[30] Z. Chang, A. Rundquist, H. Wang, I. Christov, H. C. Kapteyn, and M. M. Murnane, Phys. Rev. A **58**, R30 (1998).
[31] See Supplemental Material at http://link.aps.org/supplemental/10.1103/PhysRevLett.109.073004 for a detailed discussion of the methods used to measure the spider structures.